Effect of BaSi$_2$ template growth duration on the generation of defects and performance of p-BaSi$_2$/n-Si heterojunction solar cells

Suguru Yachi, Ryota Takabe, Tianguo Deng, Kaoru Toko, and Takashi Suemasu[*]

Institute of Applied Physics, University of Tsukuba, Tsukuba, Ibaraki 305-8573, Japan

[*]Email: suemasu@bk.tsukuba.ac.jp

Abstract

We investigated the effect of BaSi$_2$ template growth duration (t_{RDE} = 0–20 min) on the defect generation and performance of p-BaSi$_2$/n-Si heterojunction solar cells. The p-BaSi$_2$ layer grown by molecular beam epitaxy (MBE) was 15 nm thick with a hole concentration of 2×10^{18} cm^{-3}. The conversion efficiency η increased for films grown at long t_{RDE}, owing to improvements of the open-circuit voltage (V_{OC}) and fill factor (FF), reaching a maximum of η = 8.9% at t_{RDE} = 7.5 min. However, η decreased at longer and shorter t_{RDE} owing to lower V_{OC} and FF. Using deep-level transient spectroscopy, we detected a hole trap level 190 meV above the valence band maximum for the sample grown without the template (t_{RDE} = 0 min). An electron trap level 106 meV below the conduction band minimum was detected for a sample grown with t_{RDE} = 20 min. The trap densities for both films were (1–2) $\times 10^{13}$ cm^{-3}. The former originated from the diffusion of Ba into the n-Si region; the latter originated from defects in the template layer.

The crystalline qualities of the template and MBE-grown layers were discussed. The root-mean-square surface roughness of the template reached a minimum of 0.51 nm at t_{RDE} = 7.5 min. The a-axis orientation of p-BaSi$_2$ thin films degraded as t_{RDE} exceeded 10 min. In terms of p-BaSi$_2$ crystalline quality and solar cell performance, the optimum t_{RDE} was determined to be 7.5 min, corresponding to approximately 4 nm in thickness.

1. Introduction

Photovoltaic solar cells have been widely studied as an important device for the generation of electricity. The leading material used in photovoltaics is crystalline silicon (c-Si). More than 90% of installed solar cells are based on c-Si [1-3]. Yoshikawa *et al*. have recently reported a record efficiency (η) exceeding 26% [4]. However, this value of η is already close to the theoretical Shockley–Queisser limit [5]. The bandgap (E_g) of c-Si is 1.1 eV, which is smaller than the optimum E_g of approximately 1.4 eV for a single-junction solar cell. To achieve high η at a low cost, various thin-film solar cell materials, such as $Cu(In,Ga)Se_2$ [6-10], CdTe [11,12], and perovskite solar cells [13-18], have attracted considerable attention because of their higher optical absorption coefficient (α) and larger E_g than those of c-Si. However, many of these materials make use of rare and/or toxic elements. Si thin-film solar cells have also been studied; however, it is difficult to achieve η higher than 20% because of the small α value of Si [19-23]. An ideal alternative absorbing material should have a high α, a long minority-carrier lifetime, and an E_g value close to 1.4 eV. Orthorhombic barium disilicide ($BaSi_2$) has all these properties [24]. $BaSi_2$ can be grown epitaxially on a Si(111) substrate with three epitaxial variants rotated by 120° from each other around the surface normal [25]. Furthermore, $BaSi_2$ has a bandgap of 1.3 eV [26,27] and its α value is 3×10^4 cm^{-1} at 1.5 eV, which is more than 50 times larger than that of c-Si, despite the indirect bandgap of $BaSi_2$ [28,29]. Undoped n-$BaSi_2$ exhibits a minority-carrier diffusion length L of ca. 10 μm [30] and a minority-carrier lifetime of ca. 10 μs [31,32],

3

which are sufficiently large for thin-film solar cell applications. Impurity doping of $BaSi_2$ enables control over the carrier type and carrier concentration to enable the fabrication of $BaSi_2$ p-n junction diodes [33-35]. Owing to the large L and α values, a value of η greater than 25% can be expected from a 2-μm-thick $BaSi_2$ p-n junction diode [36]. Other types of solar cells such as $BaSi_2$ nanowires and $BaSi_2$/perovskite stacked layers have also been proposed [37-39].

Prior to attempting to develop a $BaSi_2$ homojunction solar cell, we fabricated p-$BaSi_2$/n-Si heterojunction solar cells and achieved a value of η approaching 10% [40-42]. This device structure represents a suitable configuration for investigating defects around the $BaSi_2$/Si heterointerface. For growth of $BaSi_2$ films on Si(111), we used a two-step growth technique. First, a very thin $BaSi_2$ template layer was grown by Ba deposition on a heated Si substrate by reactive deposition epitaxy (RDE). This template layer acted as a seed crystal for the subsequent growth of a $BaSi_2$ layer by the co-deposition of Ba and Si by molecular beam epitaxy (MBE) [25]. This thin template layer approach expands the range of material systems possible, not only for $BaSi_2$ [25] but also for other silicides, such as β-$FeSi_2$ [43,44]. Furthermore, it has been reported that the β-$FeSi_2$ template layer reduces the diffusion of Fe atoms into the Si substrate during MBE [45], implying that the template layer has a well-defined silicide/Si heterointerface, suitable for solar cell applications. However, there have been no reports to date on defects that occur at the $BaSi_2$/Si interface, induced by several factors such as the diffusion of Ba into the Si and differences in the crystal structure and lattice constants of the two layers. In this work,

we investigated the optimum template growth duration (t_{RDE}) to determine the appropriate template thickness and discuss the effect of t_{RDE} on the crystalline quality of the p-BaSi$_2$ thin films and the resulting performance of p-BaSi$_2$/n-Si heterojunction solar cells.

2. Experimental method

We used an ion-pumped MBE system (R-DEC) equipped with an electron-beam (EB) evaporation source for Si and standard Knudsen cells for Ba and B. We grew B-doped p-BaSi$_2$ epitaxial films on n-Si(111) (resistivity $\rho = 1-4$ Ω cm) to fabricate p-BaSi$_2$/n-Si heterojunction solar cells. Before the growth, the Si substrates were prepared as follows. The substrates were washed by RCA cleaning steps, including the removal of organic and metallic contaminants. The substrates were then heated at 900 °C for 30 min in ultrahigh vacuum to remove the protective SiO$_2$ layers. We first deposited Ba on a heated n-Si(111) substrate at 500 °C by RDE to form a BaSi$_2$ template layer. Next, we evaporated Ba and Si at 600 °C by MBE to form a 15-nm-thick p-BaSi$_2$ epitaxial layer. During the MBE growth, we also supplied B as a p-type dopant to ensure the hole concentration $p = 2 \times 10^{18}$ cm^{-3}. Then, we formed a 3-nm-thick amorphous Si capping layer at 180 °C to prevent the surface oxidation of p-BaSi$_2$ [46]. Finally, 80-nm-thick indium-tin-oxide (ITO) surface electrodes of 1 mm diameter and Al rear electrodes were formed by sputtering to evaluate the electrical characteristics. We fixed the MBE growth duration at 12 min (ca. 15 nm) and changed the RDE growth duration (t_{RDE}) from 0 to 20 min.

We used X-ray reflectivity (XRR) measurements to evaluate the layer thickness and the crystalline quality was characterized by reflection high-energy electron diffraction (RHEED), out-of-plane (θ-2θ) and in-plane (φ-$2\theta_\chi$) X-ray diffraction (XRD), and ω-scan X-ray rocking-curve measurements with CuKα radiation. We used a Ge(220) single crystal monochromator for the X-rays. Surface morphologies were observed by atomic force microscopy (AFM). Current density versus voltage (*J-V*) characteristics were measured under standard AM1.5, 100 mW/cm^2 illumination at 25 °C. Photoresponse spectra were measured at room temperature by a lock-in technique using a xenon lamp with a 25-cm-focal-length single monochromator (Bunko Keiki SM-1700A and RU-60N). The light intensity was calibrated with a pyroelectric sensor (Melles Griot 13PEM001/J). All measurements were performed using a mask with 1-mm-diameter holes. The deep-level transient spectroscopy (DLTS) measurements were performed in the temperature range of 80–300 K using an 1 MHz capacitance-voltage meter (HP, 4280A) to evaluate the defects [47]. The depletion region stretched into the n-Si region owing to the large difference in carrier concentration between p-BaSi$_2$ ($p = 2{\times}10^{18}$ cm^{-3}) and n-Si ($n \approx 2{\times}10^{15}$ cm^{-3}). Secondary ion mass spectrometry (SIMS) measurements were conducted with O$_2{}^+$ ion to investigate the Ba diffusion into n-Si. When the SIMS measurements were performed from the front surface side, there is a possibility that primary O$_2{}^+$ ions might push Ba atoms deeper into the n-Si side, affecting the depth profile of Ba atoms. To avoid this effect, the SIMS measurements were performed from the back surface of the n-Si substrate.

3. Results and discussion

Figure 1 shows the t_{RDE} dependence of the total measured $BaSi_2$ thickness after MBE. The gray

area corresponds to the RDE-grown layer thickness. We found that the $BaSi_2$ thickness by MBE

was approximately 15 nm in Fig. 1. The thickness increased almost linearly with t_{RDE}. The

RDE-grown thickness reached 10 nm at $t_{RDE} = 20$ min.

Figure 2(a) shows the *J-V* characteristics under AM1.5 illumination and Fig. 2(b)

shows external quantum efficiency (*EQE*) spectra for samples grown with various t_{RDE} values.

Among the various parameters, the open-circuit voltage (V_{OC}) changed considerably depending

on t_{RDE}, whereas there were no notable differences in the *EQE* spectra and thereby short-circuit

current density (J_{SC}). To discuss what happens in these devices, solar cell parameters such as

the series resistance R_S and the shunt resistance R_{SH} were derived using the following equation

[48]:

$$\frac{dV}{dJ} = SR_S + \frac{\gamma k_B T}{q} \left[\frac{1 - (SR_{SH})^{-1} dV/dJ}{J + J_{SC} - (SR_{SH})^{-1} V} \right], \qquad (1)$$

where q is the elementary charge, γ is the diode ideality factor, k_B is the Boltzmann constant, T

is the absolute temperature, and S is the device area. The solar cell parameters are summarized

in Fig. 3. The conversion efficiency η increased with t_{RDE}, reaching a maximum of 8.9% at t_{RDE}

$= 7.5$ min, before decreasing at longer t_{RDE}. The same trend was obtained for the V_{OC} and fill

factor (*FF*) as t_{RDE} was varied. The t_{RDE} of 7.5 min corresponded to an approximately 4 nm-

thick BaSi$_2$ layer, according to Fig. 1. J_{SC} gradually decreased at $t_{RDE} > 10$ min. Although R_{SH} was scattered, R_S became large at shorter and longer t_{RDE}, affecting the FF. On the basis of these results, we determined the optimum t_{RDE} to be 7.5 min (thickness of ca. 4 nm) from the viewpoint of solar cell performance.

To investigate the reasons for η degradation for small and large t_{RDE}, we performed DLTS measurements to evaluate the defect densities and their energy levels near the heterointerface. A schematic representation of the DLTS measurement is shown in Fig. 4(a). All voltages were applied to p-BaSi$_2$ with respect to n-Si. A forward filling pulse voltage (V_P) disturbs the steady-state reverse-bias condition, causing the electric field in the depletion region to decrease, which induces the defect levels to be recharged. When the voltage returns to its steady state, the defect levels begin to discharge by emitting trapped carriers through thermal emission, and the resultant time evolution of the capacitance change $S(T)$ is measured over various rate windows. DLTS allows the immediate determination of whether defects act as minority-carrier traps or majority-carrier traps from the sign of the DLTS signal. Positive signals indicate the presence of minority-carrier traps, and negative signals indicate the presence of majority-carrier traps. Figures 4(b)(b′)−4(d)(d′) show the DLTS spectra of the p-BaSi$_2$/n-Si heterojunction solar cells grown with $t_{RDE} = 0$, 7.5, and 20 min. We set V_P at 1 V with a pulse width of 50 ms. A reversed-biased voltage (V_R) was set at −3 V in Figs. 4(b)−4(d), and −0.01 V in Figs. 4(b′)−4(d′). The rate window was 0.5−128 ms. At $V_R = −3$ V, the depletion

region stretched approximately 1.5 μm from the interface towards the n-Si side; however, it remained close to the heterointerface at $V_R = -0.01$ V. We detected one minority carrier (hole) trap (H1) in the $t_{RDE} = 0$ min film, as shown in Fig. 4(b), and a majority carrier (electron) trap (E1) in the $t_{RDE} = 20$ min film, shown in Fig. 4(d′), explaining the degradation of η for small and large t_{RDE}. No other distinct defects were observed. Figure 5 shows Arrhenius plots of these two traps H1 and E1. The hole trap level H1 was located 190 meV above the valence band maximum (VBM), and the trap density was $N_T^h = 2.2 \times 10^{13}$ cm^{-3}. The electron trap level E1 was located 106 meV below the conduction band minimum (CBM), and the trap density was $N_T^e = 1.5 \times 10^{13}$ cm^{-3} for E1. The DLTS measurements revealed that the samples without the BaSi$_2$ template ($t_{RDE} = 0$ min) featured a hole trap level H1 in the n-Si bulk region, and that film growth based on the thickest BaSi$_2$ template ($t_{RDE} = 20$ min) featured an electron trap level E1 near the heterointerface.

Figure 6 shows the SIMS depth profiles of Ba and Si atoms of the samples grown with $t_{RDE} = 1$ and 10 min. The plots in red show the profiles of Ba atoms and the black plots denote those of Si atoms. Reference samples with a controlled number of Ba atoms doped in Si have yet to be prepared. Hence, we used the SIMS signal intensity to compare these two samples. At a depth > 60 nm, the SIMS intensity in the sample grown with $t_{RDE} = 1$ min was almost one order of magnitude larger than that in the sample grown with $t_{RDE} = 10$ min. We can therefore assume that the diffusion of Ba atoms into the n-Si was suppressed in the sample grown with

$t_{RDE} = 10$ min compared with that for the sample grown with $t_{RDE} = 1$ min. Thus, the RDE-grown template acts as a diffusion barrier for Ba atoms, as is the case in β-FeSi$_2$ [45]. We therefore ascribe the hole trap level (H1), observed in Fig. 4(b), to the diffusion of Ba atoms into n-Si.

To understand why the diffusion of Ba atoms into the Si substrate was promoted for the template at $t_{RDE} = 1$ min, we observed the surface morphologies of the RDE-grown layers. Figure 7 shows AFM topographic images (2×2 μm^2) of the RDE-grown BaSi$_2$ surfaces grown at (a) $t_{RDE} = 1$ min, (b) $t_{RDE} = 7.5$ min, and (c) $t_{RDE} = 15$ min. The cross-sectional profiles along the broken lines are also shown. The root-mean-square (RMS) roughness values of the RDE-grown BaSi$_2$ were 0.74, 0.42, and 1.58 nm at $t_{RDE} = 1$, 7.5, and 15 min, respectively. The smallest value was obtained at $t_{RDE} = 7.5$ min. We found a large number of small BaSi$_2$ islands on the Si(111) surface at $t_{RDE} = 1$ min in Fig. 7(a), indicating that the template did not cover the entire Si surface. Hence, p-BaSi$_2$ was directly grown on a large part of the Si(111) surface by MBE. The diffusion of Ba atoms into the Si substrate is promoted at higher temperatures. In this study, RDE and MBE growths were conducted at 500 and 600 °C, respectively. Hence, it can be safely stated that Ba diffusion during MBE is suppressed by a continuous template layer, as indicated by the SIMS profile in Fig. 6. As t_{RDE} was increased further to 7.5 min, the entire surface of the Si became covered with the BaSi$_2$ template, as shown in Fig. 7(b). Once the Si surface was covered with the BaSi$_2$ template at 500 °C, the diffusion of Ba atoms into Si was

likely to be suppressed even during the subsequent MBE growth at 600 °C. When t_{RDE} was

increased further to 15 min, the RMS value increased considerably to 1.58 nm, and many

valleys with depths of approximately 2 nm appeared on the template, as seen in Fig. 7(c).

We next consider the origin of the E1 level detected at $V_R = -0.01$ V for the sample

grown with $t_{RDE} = 20$ min in Fig. 4(d′). The electrical properties of the RDE-grown BaSi$_2$

template are unclear; however, it is reasonable to assume that some portion of the depletion

region stretched toward the undoped RDE-grown template at $V_R = -0.01$ V, because the RDE-

grown BaSi$_2$ thickness was approximately 10 nm at $t_{RDE} = 20$ min in Fig. 1. The RDE-grown

BaSi$_2$ template was considered to have n-type conductivity because undoped BaSi$_2$ often

presents n-type properties with an electron concentration of approximately 10^{16} cm^{-3} [26,49].

Figure 7(c) shows that the surface of the BaSi$_2$ template at $t_{RDE} = 20$ min was very rough. We

attribute such a rough surface to the supply of Si atoms from the Si substrate being deficient as

the BaSi$_2$ thickness increased. Kumar *et al*. demonstrated by first-principles calculation that Si

vacancy is a predominant defect in BaSi$_2$ [50]. Thereby, the E1 level can be interpreted to

originate from Si point defects induced in the template at $t_{RDE} = 20$ min.

Because of the differences in the carrier concentrations of p-BaSi$_2$ and n-Si, the

depletion region did not stretch toward the p-BaSi$_2$ region at $V_R < 0$, and thus the

characterization of defects was limited to the region near the interface and the n-Si bulk in the

present DLTS measurements. Here, we discuss the effect of the crystalline quality of the

11

template on the MBE-grown overlayers. Figure 8(a) shows the RMS surface roughness values of the grown p-BaSi$_2$ films as a function of t_{RDE}, and Fig. 8(b) shows the full widths at half maximum (FWHMs) of the BaSi$_2$ (600) diffraction intensity as a function of t_{RDE}. The RMS decreased as t_{RDE} was increased and became a minimum at approximately $t_{RDE} = 6.5, 7.5$, and 10 min, and then increased. This trend was almost the same as that of an RDE-grown BaSi$_2$ template, as shown in Fig. 7. We speculate that there is a possibility that such rough surfaces of p-BaSi$_2$ might increase R_S because of insufficient contact between ITO and p-BaSi$_2$ for samples grown at shorter and longer t_{RDE}, leading to the decrease in FF as shown in Fig. 3. The FWHM increased with t_{RDE}, most notably for $t_{RDE} > 10$ min, indicating that the crystal orientation degraded as t_{RDE} was prolonged. Thus, a t_{RDE} of 6.5−10 min is optimal from the viewpoint of p-BaSi$_2$ crystalline quality. These results suggest that the increase in FWHM with t_{RDE} is related to the lattice relaxation of BaSi$_2$. Both the out-of-plane and in-plane lattice constants were calculated from the peak positions in the θ-2θ and φ-$2\theta_\chi$ XRD patterns, respectively. Measurement errors were minimized with the use of the Nelson–Riley equation for the calculations [51]. Figures 9(a)−9(c) show the dependence of BaSi$_2$ a-, b-, and c-axis lattice constants of BaSi$_2$ films on t_{RDE}, respectively. The in-plane epitaxial relationships of a-axis-oriented BaSi$_2$ on Si(111) were BaSi$_2$[010]//Si[11$\overline{2}$] and BaSi$_2$[001]//Si[$\overline{1}$10]. The blue broken lines show the lattice constants of BaSi$_2$ bulk [52], the broken red line in Fig. 9(b) shows the interplanar distance of Si(11$\overline{2}$), and the broken green line in Fig. 9(c) denotes three times the

interplanar distance of Si(110) [25]. The lattice constants b and c of the BaSi$_2$ films almost lattice-matched with the Si(111) surface for short t_{RDE}, meaning that BaSi$_2$ was under in-plane compressive strain. As t_{RDE} was increased, BaSi$_2$ relaxed, and the measured lattice constants a, b, and c approached the bulk BaSi$_2$ values. These results show that BaSi$_2$ films at short t_{RDE} were strained and their lattices became relaxed as t_{RDE} was increased. In terms of both solar cell performance and the crystalline quality of p-BaSi$_2$, we conclude that the optimum template thickness was approximately 4 nm ($t_{RDE} = 7.5$ min).

4. Conclusions

We fabricated p-BaSi$_2$/n-Si heterojunction solar cells and investigated the effect of t_{RDE} on defect formation and solar cell performance. The value of η increased as t_{RDE} increased because of the improvements of V_{OC} and FF. The maximum value was $\eta = 8.9\%$ from a film grown with $t_{RDE} = 7.5$ min. We detected one hole trap (H1) located 190 meV above the VBM with $N_T^h =$ 2.2×10^{13} cm^{-3} in the n-Si side of the sample grown without the template ($t_{RDE} = 0$ min). In addition, one electron trap (E1) was located 106 meV below the CBM with $N_T^e = 1.5 \times 10^{13}$ cm^{-3}, which was likely present in the RDE-grown template for the sample grown with a long t_{RDE} of 20 min. The H1 and E1 traps were attributed to the diffusion of Ba atoms into the n-Si and the degraded RDE template layer, respectively. On the basis of these results, the optimum t_{RDE} was determined to be 7.5 min (ca. 4 nm) from the viewpoints of both solar cell performance

and crystalline quality of the p-BaSi$_2$ films.

Acknowledgments

[1] S. R. Wenham and M. A. Green, Prog. Photovoltaics **4**, 3 (1996).

[2] M. A. Green, Prog. Photovoltaics **17**, 183 (2009).

[3] V. V. Tyagi, N. A. A. Rahim, N. A. Rahim, and J. A. L. Selvaraj, Renewable Sustainable

Energy Rev. **20**, 443 (2013).

[4] K. Yoshikawa, H. Kawasaki, W. Yoshida, T. Irie, K. Konishi, K. Nakano, T. Uto, D. Adachi,

M. Kanematsu, H. Uzu, and K. Yamamoto, Nat. Energy **2**, 17302 (2017).

[5] W. Shockley, W. Hans, and H. J. Queisser, J. Appl. Phys. **32**, 510 (1961).

[6] P. Jackson, D. Hariskos, R. Wuerz, O. Kiowski, A. Bauer, T. M. Friedlmeier, and M. Powalla,

Phys. Status Solidi RL **9**, 28 (2015).

[7] P. Jackson, D. Hariskos, E. Lotter, S. Paetel, R. Wuerz, R. Menner, W. Wischmann, and M.

Powalla, Prog. Photovoltaics **19**, 894 (2011).

[8] S. C. Riha, B. A. Parkinson, and A. L. Prieto, J. Am. Chem. Soc. **131**, 12054 (2009).

[9] M. G. Panthani, V. Akhavan, B. Goodfellow, J. P. Schmidtke, L. Dunn, A. Dodabalapur, P.

F. Barbara, and B. A. Korgel, J. Am. Chem. Soc. **130**, 16770 (2008).

[10] I. Repins, M. A. Contreras, B. Egaas, C. DeHart, J. Scharf, C. L. Perkins, B. To, and R.

Noufi, Prog. Photovoltaics **16**, 235 (2008).

[11] S. Kim, B. Fisher, H. J. Eisler, and M. Bawendi, J. Am. Chem. Soc. **125**, 11466 (2003).

[12] J. Britt and C. Ferelides, Appl. Phys. Lett. **62**, 2851 (1993).

[13] J. Burschka, N. Pellet, S. J. Moon, R. H. Baker, P. Gao, M. K. Nazeeruddin, and M. Grätzel,

Nature **499**, 316 (2013).

[14] M. Liu, M. B. Johnston, and H. J. Snaith, Nature **501**, 395 (2013).

[15] S. D. Stranks, G. E. Eperon, G. Grancini, C. Menelaou, M. J. P. Alcocer, T. Leijtens, L. M. Herz, A. Petrozza, and H. J. Snaith, Science **342**, 341 (2013).

[16] M. M. Lee, J. Teuscher, T. Miyasaka, T. N. Murakami, and H. J. Snaith, Science **338**, 643 (2012).

[17] H. S. Kim, C. R. Lee, J. H. Im, K. B. Lee, T. Moehl, A. Marchioro, S. J. Moon, R. H. Baker, J. H. Yum, J. E. Moser, M. Grätzel, and N. G. Park, Sci. Rep. **2**, 591 (2012).

[18] A. Kojima, K. Teshima, Y. Shirai, and T. Miyasaka, J. Am. Chem. Soc. **131**, 6050 (2009).

[19] T. Matsui, H. Sai, K. Saito, and M. Kondo, Prog. Photovoltaics **21**, 1363 (2013).

[20] J. Müller, B. Rech, J. Springer, and M. Vanecek, Sol. Energy **77**, 917 (2004).

[21] K. L. Chopra, P. D. Paulson, and V. Dutta, Prog. Photovoltaics **12**, 69 (2004).

[22] A.V. Shah, H. Schade, M. Vanecek, J. Meier, E.V. Sauvain, N. Wyrsch, U. Kroll, C. Droz, and J. Bailat, Prog. Photovoltaics **12**, 113 (2004).

[23] A. Shah, P. Torres, R. Tscharner, N. Wyrsch, and H. Keppner, Science **285**, 692 (1999).

[24] T. Suemasu and N. Usami, J. Phys. D **50**, 023001 (2017).

[25] Y. Inomata, T. Nakamura, T. Suemasu, and F. Hasegawa, Jpn. J. Appl. Phys. **43**, L478 (2004).

[26] K. Morita, Y. Inomata, and T. Suemasu, Thin Solid Films **508**, 363 (2006).

[27] K. Toh, T. Saito, and T. Suemasu, Jpn. J. Appl. Phys. **50**, 068001 (2011).

[28] M. Kumar, N. Umezawa, and M. Imai, J. Appl. Phys. **115**, 203718 (2014).

[29] D. B. Migas, V. L. Shaposhnikov, and V. E. Borisenko, Phys. Status Solidi B **244**, 2611 (2007).

[30] M. Baba, K. Toh, K. Toko, N. Saito, N. Yoshizawa, K. Jiptner, T. Sekiguchi, K. O. Hara, N. Usami, and T. Suemasu, J. Cryst. Growth **348**, 75 (2012).

[31] K. O. Hara, N. Usami, K. Nakamura, R. Takabe, M. Baba, K. Toko, and T. Suemasu, Appl. Phys. Express **6**, 112302 (2013).

[32] K. O. Hara, N. Usami, K. Toh, M. Baba, K. Toko, and T. Suemasu, J. Appl. Phys. **112**, 083108 (2012).

[33] M. Kobayashi, Y. Matsumoto, Y. Ichikawa, D. Tsukada, and T. Suemasu, Appl. Phys. Express **1**, 051403 (2008).

[34] M. A. Khan, K. O. Hara, W. Du, M. Baba, K. Nakamura, M. Suzuno, K. Toko, N. Usami, and T. Suemasu, Appl. Phys. Lett. **102**, 112107 (2013).

[35] M. A. Khan, K. Nakamura, W. Du, K. Toko, N. Usami, and T. Suemasu, Appl. Phys. Lett. **104**, 252104 (2014).

[36] T. Suemasu, Jpn. J. Appl. Phys. **54**, 07JA01 (2015).

[37] A. Pokhrel, L. Samad, F. Meng, and S. Jin, Nanoscale **7**, 17450 (2015).

[38] R. Vismara, O. Isabella, and M. Zeman, SPIE **9898**, 98980J (2016).

[39] R. Vismara, O. Isabella, and M. Zeman, Opt. Express **25**, A402 (2017).

[40] S. Yachi, R. Takabe, K. Toko, and T. Suemasu, Jpn. J. Appl. Phys. **56**, 05DB03 (2017).

[41] S. Yachi, R. Takabe, H. Takeuchi, K. Toko, and T. Suemasu, Appl. Phys. Lett. **109**, 072103 (2016).

[42] D. Tsukahara, S. Yachi, H. Takeuchi, R. Takabe, W. Du, M. Baba, Y. Li, K. Toko, N. Usami, and T. Suemasu, Appl. Phys. Lett. **108**, 152101 (2016).

[43] R. Kuroda, Z. Liu, Y. Fukuzawa, Y. Suzuki, M. Osamura, S. Wang, N. Otogawa, T. Ootsuka, T. Mise, Y. Hoshino, Y. Nakayama, H. Tanoue, and Y. Makita, Thin Solid Films **461**, 34 (2004).

[44] M. Takauji, N. Seki, T. Suemasu, F. Hasegawa, and M. Ichida, J. Appl. Phys. **96**, 2561 (2004).

[45] Z. Liu, Y. Suzuki, M. Osamura, T. Ootsuka, T. Mise, R. Kuroda, H. Tanoue, Y. Makita, S. Wang, Y. Fukuzawa, N. Otogawa, and Y. Nakayama, J. Appl. Phys. **95**, 4019 (2004).

[46] R. Takabe, S. Yachi, W. Du, D. Tsukahara, H. Takeuchi, K. Toko, and T. Suemasu, AIP Adv. **6**, 085107 (2016).

[47] D. V. Lang, J. Appl. Phys. **45**, 3023 (1974).

[48] J. R. Sites and P. H. Mauk, Sol. Cells **27**, 411 (1989).

[49] W. Du, M. Baba, K. Toko, K.O. Hara, K. Watanabe, T. Sekiguchi, N. Usami, and T. Suemasu, J. Appl. Phys. **115**, 223701 (2014).

[50] M. Kumar, N. Umezawa, W. Zhou, and M. Imai, J. Mater. Chem. A **5**, 25293 (2017).

[51] J. B. Nelson and D. P. Riley, Proc. Phys. Soc. **57**, 160 (1945).

[52] H. Schäfer, K. H. Janzou, and A. Weiss, Angew. Chem., Int. Ed. **2**, 393 (1963).

Figure captions

Fig. 1. Dependence of BaSi$_2$ layer thickness on RDE growth duration (t_{RDE} = 0, 1, 5, 6.5, 7.5, 10, 15, and 20 min), while the MBE growth duration was fixed at 12 min.

Fig. 2. (a) *J-V* characteristics of RDE films grown for various durations (t_{RDE} = 0, 1, 5, 6.5, 7.5, 10, 15, and 20 min) measured under AM1.5 illumination. (b) *EQE* spectra of films grown for various t_{RDE} values.

Fig. 3. Solar cell parameters: conversion efficiency (η), open-circuit voltage (V_{OC}), short-circuit current (J_{SC}), fill factor (*FF*), series resistance (R_S), and shunt resistance (R_{SH}) as a function of RDE growth duration (t_{RDE} = 0, 1, 5, 6.5, 7.5, 10, 15, and 20 min).

Fig. 4. (a) Principle of DLTS method and (b) DLTS spectra of p-BaSi$_2$/n-Si solar cells grown with t_{RDE} = 0, 7.5, and 20 min (b)–(d) at V_R = −3 V and (b)–(d′) at V_R = −0.01 V. The V_P was set at 1 V with a pulse width of 50 ms. The depletion region stretches mainly toward the n-Si region because of the difference in carrier concentration between p-BaSi$_2$ and n-Si.

Fig. 5. Arrhenius plots of H1 and E1 levels observed in Fig. 4.

Fig. 6. SIMS depth profiles of Ba (red) and Si (black) atoms in samples grown with $t_{RDE} = 1$ and 10 min.

Fig. 7. Topographic AFM views ($2 \times 2\ \mu m^2$) and cross-sectional profiles (along white broken lines) of RDE-grown BaSi$_2$ surfaces at (a) $t_{RDE} = 1$, (b) $t_{RDE} = 7.5$, and (c) $t_{RDE} = 15$ min. The RMS surface roughness values are presented.

Fig. 8. (a) Dependence of p-BaSi$_2$ RMS surface roughness on t_{RDE}. The RMS value became a minimum at $t_{RDE} \approx 7.5-10$ min. (b) Dependence of FWHM of BaSi$_2$ (600) intensity on t_{RDE}. The solid lines are a guide to the eyes.

Fig. 9. (a)-(c) Dependence of BaSi$_2$ lattice constants a, b, and c, respectively, on t_{RDE}. The broken blue lines show the lattice constants of bulk BaSi$_2$ [52]. The broken red and blue lines denote the interplanar distance of Si(11$\overline{2}$) and three times the interplanar distance of Si(110), respectively.
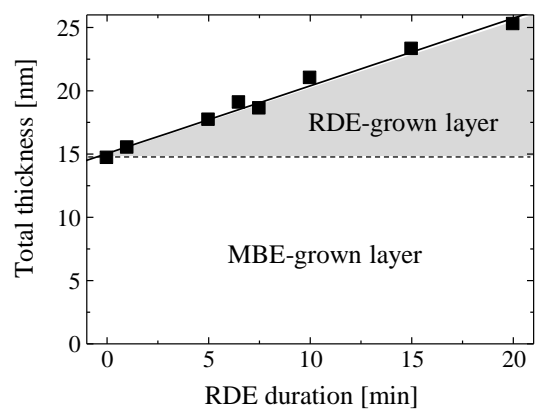
Fig. 1

(a)

(b)

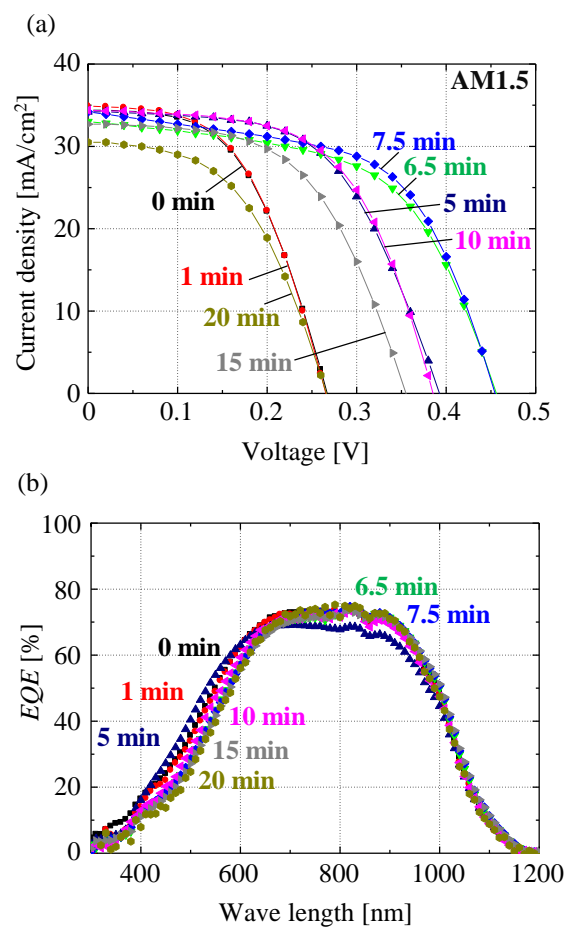Fig. 2
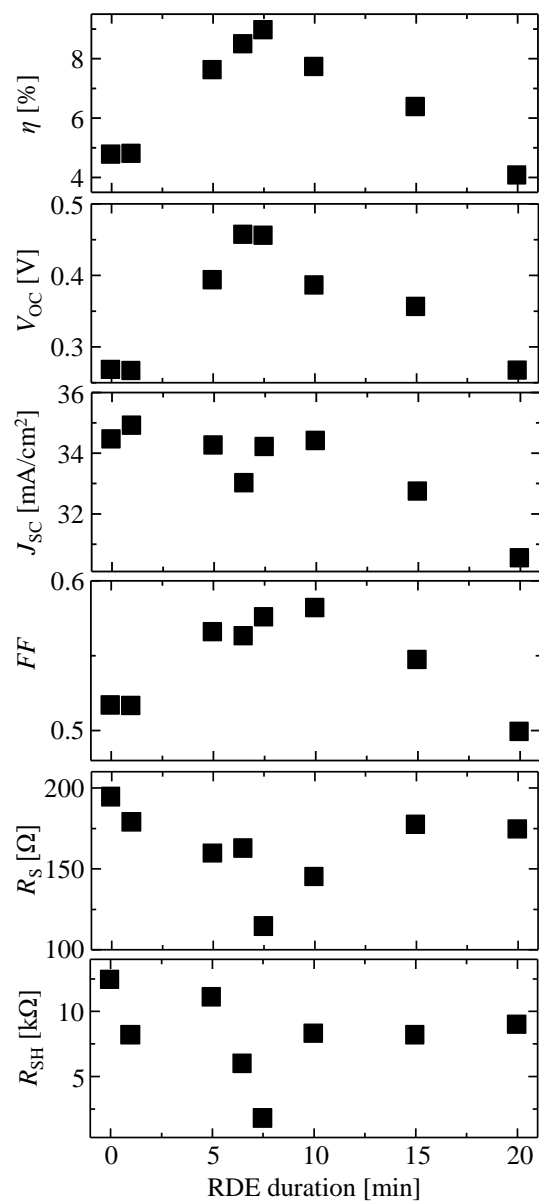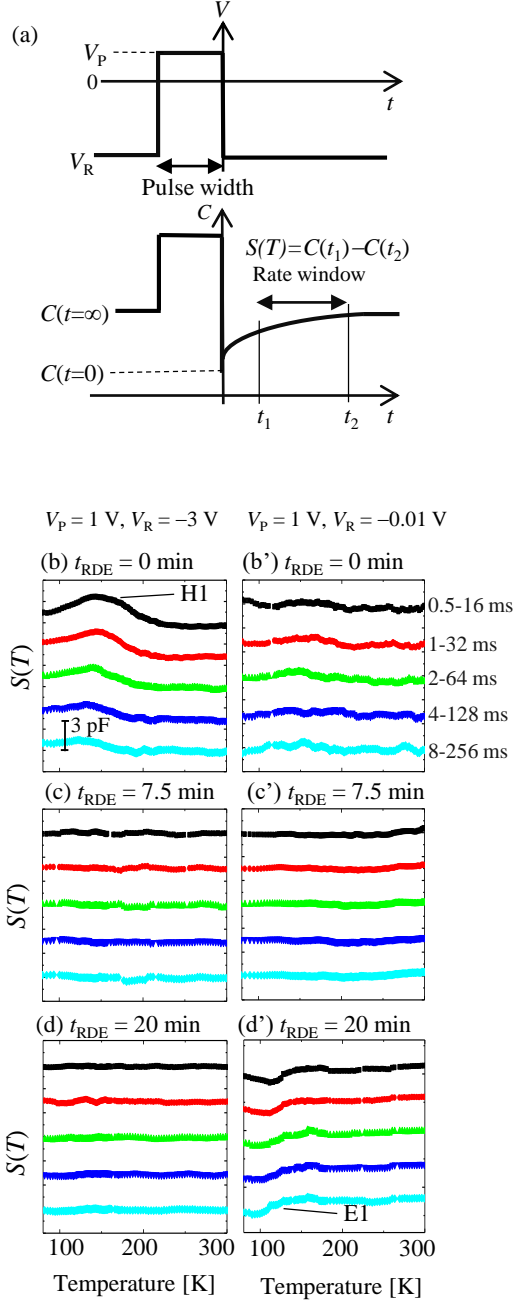
Fig. 3

(a)

V_P
0
V_R
Pulse width

C
$S(T)=C(t_1)-C(t_2)$
Rate window
$C(t=\infty)$
$C(t=0)$
t_1 t_2 t

$V_P = 1$ V, $V_R = -3$ V $V_P = 1$ V, $V_R = -0.01$ V

(b) $t_{RDE} = 0$ min   (b') $t_{RDE} = 0$ min

H1

$S(T)$

3 pF

0.5-16 ms
1-32 ms
2-64 ms
4-128 ms
8-256 ms

(c) $t_{RDE} = 7.5$ min   (c') $t_{RDE} = 7.5$ min

$S(T)$

(d) $t_{RDE} = 20$ min   (d') $t_{RDE} = 20$ min

$S(T)$

E1

100   200   300   100   200   300
Temperature [K]   Temperature [K]

Fig. 4

Fig. 5

Fig. 6

(a) RMS : 0.74 nm

1 μm

5.8 [nm]

0

(b) RMS : 0.42 nm

1 μm

3.6 [nm]

0

(c) RMS : 1.58 nm

1 μm

9.3 [nm]

0

Fig. 7

(a)

(b)

Fig. 8

(a) *a*-axis

(b) *b*-axis

(c) *c*-axis

Fig. 9